Research Article

# Cryo-EM structure of the trehalose monomycolate transporter, MmpL3, reconstituted into peptidiscs

Julie Couston [a], Zongxin Guo [b], Kaituo Wang [b], Pontus Gourdon [b,c,**], Mickaël Blaise [a,*]

[a] IRIM, CNRS, University of Montpellier, Montpellier, France
[b] Department of Biomedical Sciences, Faculty of Health and Medical Sciences, University of Copenhagen, DK-2200, Copenhagen N, Denmark
[c] Department of Experimental Medical Science, Faculty of Medicine, Lund University, SE-22100, Lund, Sweden

## ARTICLE INFO

## ABSTRACT

Mycobacteria have an atypical thick and waxy cell wall. One of the major building blocks of such mycomembrane is trehalose monomycolate (TMM). TMM is a mycolic acid ester of trehalose that possesses long acyl chains with up to 90 carbon atoms. TMM represents an essential component of mycobacteria and is synthesized in the cytoplasm, and then flipped over the plasma membrane by a specific transporter known as MmpL3. Over the last decade, MmpL3 has emerged as an attractive drug target to combat mycobacterial infections. Recent three-dimensional structures of MmpL3 determined by X-ray crystallography and cryo-EM have increased our understanding of the TMM transport, and the mode of action of inhibiting compounds. These structures were obtained in the presence of detergent and/or in a lipidic environment. In this study, we demonstrate the possibility of obtaining a high-quality cryo-EM structure of MmpL3 without any presence of detergent through the reconstitution of the protein into peptidiscs. The structure was determined at an overall resolution of 3.2 Å and demonstrates that the overall structure of MmpL3 is preserved as compared to previous structures. Further, the study identified a new structural arrangement of the linker that fuses the two subdomains of the transmembrane domain, suggesting the feature may serve a role in the transport process.

## 1. Introduction

Mycobacteria are gram-positive bacteria that can be pathogenic for humans. *Mycobacterium tuberculosis* (*Mtb*) belongs to this genus and is the etiologic agent of tuberculosis (TB). In 2021, it was estimated that TB was responsible for 1.6 million deaths and 10.6 million new infections (WHO, 2022). The mycobacterial cell wall named mycomembrane is complex and thick and comprises a wide panel of lipids and glycolipids (Dulberger et al., 2020). Among these, trehalose monomycolate (TMM) is a central building block for the mycomembrane. TMM is synthesized in the cytoplasmic compartment and is then flipped across the inner membrane by the MmpL3 transporter where it can integrate the mycomembrane and/or can be converted into trehalose dimycolate (Marrakchi et al., 2014; Quémard, 2016). The Mycobacterial membrane protein Large family (MmpL) is involved in drug-efflux and export of the different lipids and glycolipids in mycobacteria (Viljoen et al., 2017). Notably, the mycolic acid pathway is essential for mycobacterial survival and it is, therefore, a target of several inhibitors used to treat mycobacterial infections (Abrahams and Besra, 2018). The emergence of multiple, extremely or totally drug-resistant mycobacterial strains however urges to find new molecules to assist the current therapeutic arsenal and counteract these worrisome drug resistant strains (WHO, 2022). MmpL3, the TMM transporter, whose function was discovered a decade ago (Grzegorzewicz et al., 2012; Tahlan et al., 2012) is a member of the large resistance-nodulation-division (RND) and shares a similar topology with efflux pumps of this family class, in terms of number of transmembrane helices and periplasmic domains (Fig. 1A) (Alav et al., 2021; Nikaido, 2018). Importantly, MmpL3 has emerged as an interesting drug target to combat *Mtb* infections but also other notoriously difficult to treat non-tuberculous mycobacteria such as *Mycobacterium abscessus* (Dupont et al., 2016). Indeed, numerous newly discovered and diverse inhibitors targeting MmpL3 show great promise as new anti-mycobacterial compounds (North et al., 2023).

The recent progress in the biochemical and structural investigations

* Corresponding author. IRIM, CNRS, University of Montpellier, Montpellier, France.
** Corresponding author. Department of Biomedical Sciences, Faculty of Health and Medical Sciences, University of Copenhagen, DK-2200, Copenhagen N, Denmark.
E-mail addresses: pontus@sund.ku.dk (P. Gourdon), mickael.blaise@irim.cnrs.fr (M. Blaise).

of MmpL3 brought important fundamental knowledge on TMM transport. Activity assays in spheroplasts and reconstitution of MmpL3 in proteoliposomes have confirmed the role of MmpL3 in TMM flipping (Xu et al., 2017) and that TMM transport is coupled to a proton gradient as seen for other RND pumps (Stevens et al., 2022). Three-dimensional structures of the apo forms of MmpL3 solved either by X-ray crystallography or cryo-EM as well as in complex with TMM or MmpL3 inhibitors shed light on the mechanism of TMM transport and its inhibition. To date sixteen three-dimensional structures of MmpL3 from *Mycobacterium smegmatis* (hereafter MmpL3$_{Msm}$) were solved of which nine were determined by X-ray crystallography and seven by cryo-EM, all of the latter were reconstituted in lipid nanodiscs (Hu et al., 2022; Su et al., 2019, 2021; Yang et al., 2020; Zhang et al., 2019). One additional MmpL3 structure from *Mtb* was solved by cryo-EM (Adams et al., 2021). Thus far, all MmpL3 structures lack the 30 kDa C-terminal domain which is not essential for the transport function (Stevens et al., 2022). Further, all the MmpL3$_{Msm}$ X-ray structures were obtained using the same detergent namely n-dodecyl-β-D-maltopyranoside (DDM) or purified in DDM and then inserted in lipid nanodiscs for cryo-EM purposes. Only MmpL3 from *Mtb* was purified in another detergent than DDM namely Lauryl Maltose Neopentyl Glycol (LMNG) and its structure was determined by cryo-EM in the same detergent (Adams et al., 2021).

We recently succeeded to stabilize MmpL3$_{Msm}$ in other detergents than DDM, including in sodium deoxycholate (Ung et al., 2022a). Of interest, we were also able to reconstitute MmpL3$_{Msm}$ into peptidiscs. This approach offers the possibility to stabilize membrane proteins in the absence of detergent or any addition of lipids as compared to the

nanodisc (Carlson et al., 2018; Denisov and Sligar, 2017) or Salipro (Frauenfeld et al., 2016) technologies and without tedious assessment of the type of scaffolds and lipids as well as of the lipid to protein ratios. Moreover, peptidiscs are compatible with structural biology approaches (Angiulli et al., 2020), including single particle cryo-EM, as recently also shown for relatively small membrane proteins (Ung et al., 2022b). In this study, we report that the reconstitution of MmpL3$_{Msm}$ into peptidiscs allows its structural determination using single particle cryo-EM.

## 2. Materials and methods

### 2.1. Protein expression, solubilization and purification

The expression and purification of MmpL3$_{Msm}$ were essentially performed as described previously (Ung et al., 2022a). The construct was made of two amplicons of codon-optimized *mmpL3$_{Msm}$* (amino acids 1–773) and *mmpL3$_{Msm}$* (amino acids 774–1013), inserted around a Tobacco Etch Virus (TEV) protease cleavage site and a polyhistidine tag (8xHis) (Fig. 1B). 500 ng of plasmid were transformed into chemically competent *E. coli* C43 Δ*acrB* strain. An overnight preculture was used to initiate a 12 L culture in LB media supplemented with ampicillin. Protein expression was induced with 1 mM isopropyl β-D-1-thiogalactopyranoside (IPTG, Euromedex) for 3 h at 37 °C. Bacteria were harvested for 15 min at 8,000 *g* and 4 °C, then resuspended in buffer A (20 mM Tris-HCl pH 8, 150 mM NaCl, 1 mM benzamidine, 10 % (v/v) glycerol, 0.5 mM β-mercaptoethanol) and stored at −20 °C until further use.

Bacteria were thawed in water and the solution was supplemented
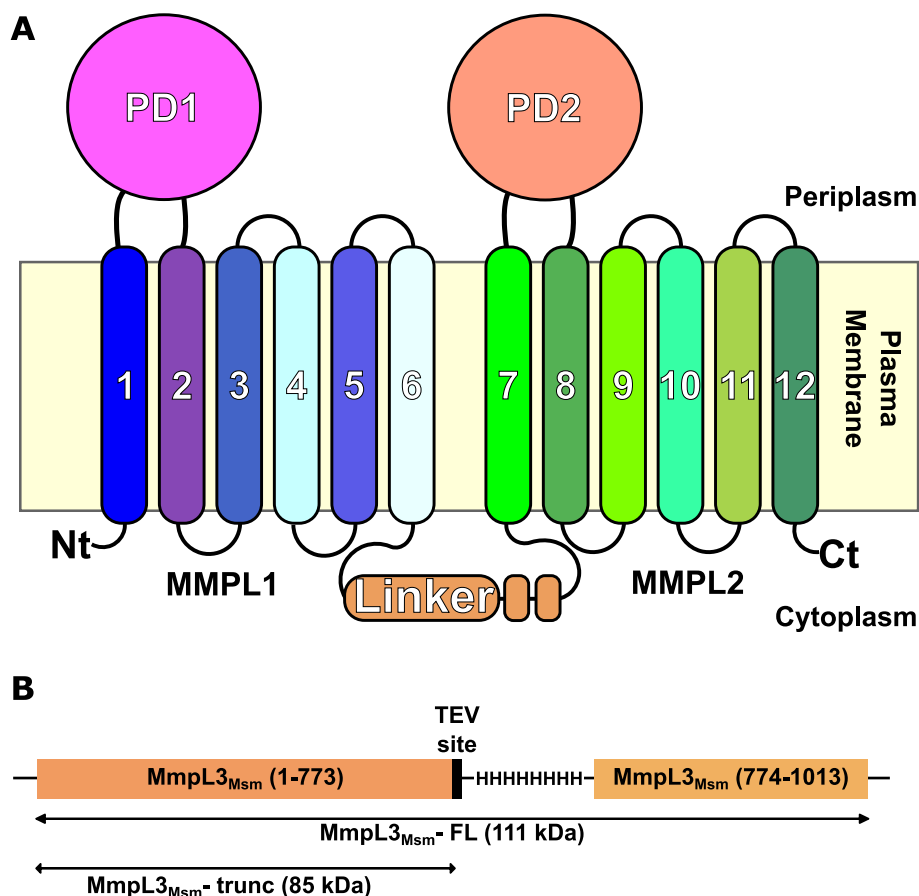


**Fig. 1.** Schematic of MmpL3$_{Msm}$

A-Two-dimensional diagram, showing MMPL1 (TM1 to 6) and MMPL2 (TM7 to 12) domains separated by the linker region. The two periplasmic domains 1 and 2 (PD1 and PD2) are located in-between TM1 and 2 and TM7 and 8, respectively. Nt and Ct stand for N-terminus and C-terminus. The color code is the same as in Fig. 5. B-Construct design used to express MmpL3$_{Msm}$. (For interpretation of the references to color in this figure legend, the reader is referred to the Web version of this article.)

with a tablet of protease inhibitor cocktail (Sigma). All subsequent steps were performed at 4 °C. Bacteria were lysed by sonication (Digital Sonifier, Branson) during 4 cycles of 2 min each, composed of 2 s pulse followed by 2 s pause, at 40 % intensity. The solution was clarified by centrifugation for 45 min at 28,000 *g*. The supernatant containing soluble material was further ultracentrifuged (Optima XE ultracentrifuge, Beckman Coulter) for 2 h 30 at 185,000 *g*, using a Ti 50.2 rotor (Beckman Coulter). The supernatant was discarded and membrane fractions were resuspended by Dounce homogenization in buffer B (20 mM Tris-

HCl pH 8, 1 M NaCl, 1 mM benzamidine, 10 % (v/v) glycerol, 0.5 mM $\beta$-mercaptoethanol), then ultracentrifuged a second time in the same conditions. The next day, membranes were resuspended in 80 mL of buffer C (20 mM Tris-HCl pH 8, 150 mM NaCl, 1 mM benzamidine, 10 % (v/v) glycerol, 0.5 mM $\beta$-mercaptoethanol, 20 mM imidazole) and protein solubilized with 1 % (w/v) of *n*-Dodecyl-$\beta$-D-Maltopyranoside (DDM) detergent (Anatrace) for 2 h. The solution was then ultracentrifuged for 1 h at 185,000 *g*. Protein purification was first performed by two steps of immobilized metal affinity chromatography (IMAC).
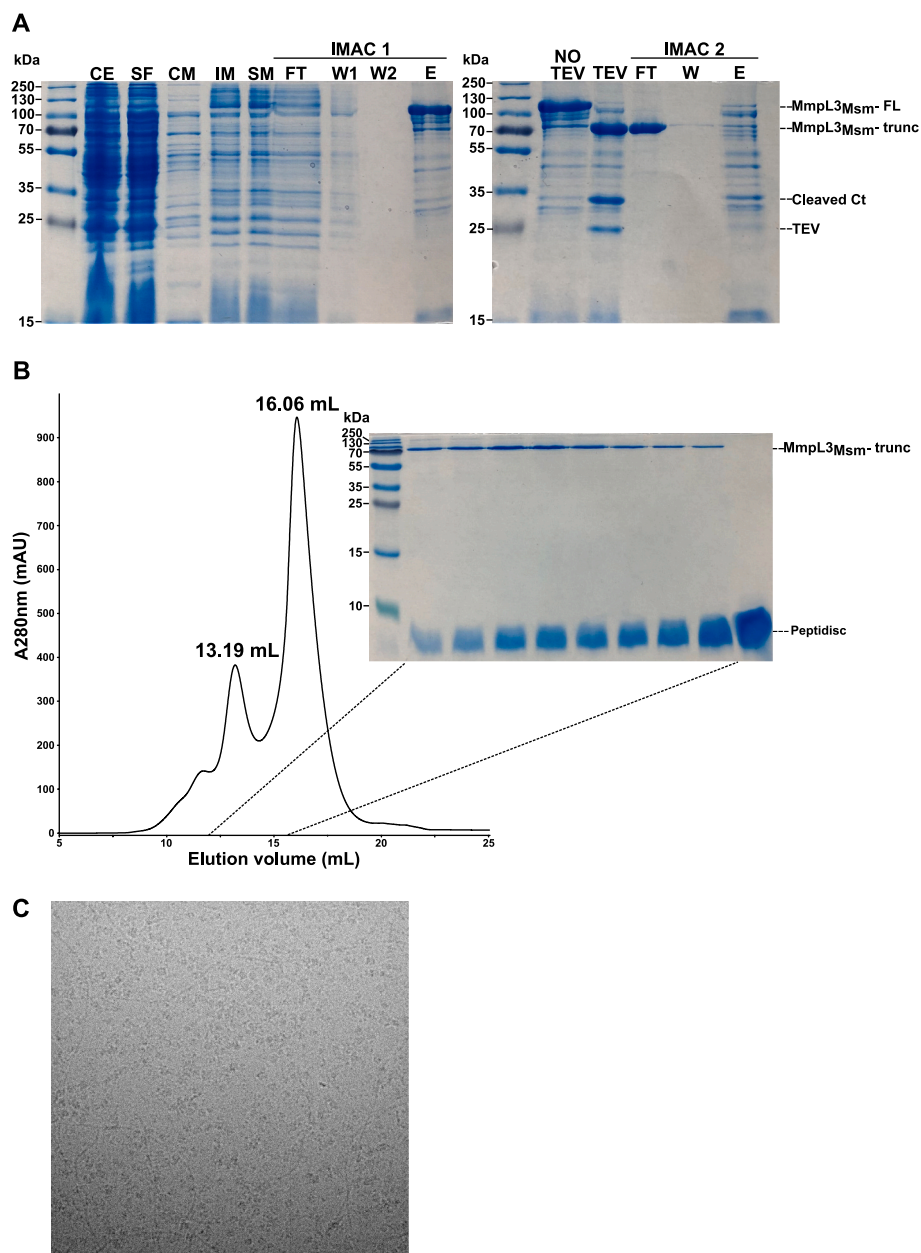


**Fig. 2.** Expression, purification and reconstitution of MmpL3$_{Msm}$ into peptidiscs for cryo-EM investigation

**A**-Purification steps of MmpL3$_{Msm}$ on Coomassie-stained SDS-PAGE. The shift of the protein molecular weight from ~110 kDa to ~85 kDa corresponds to TEV cleavage. CE, crude extract: sample after bacterial lysis obtained by sonication; SF, soluble fraction: lysed fraction after centrifugation, containing soluble proteins; CM, crude membranes: supernatant after ultracentrifugation 1 and 2; IM, insoluble membranes: resuspended pellet after ultracentrifugation 1 and 2; SM, soluble membranes: supernatant from ultracentrifugation 3, containing insoluble membranes in solution after addition of 1 % (w/v) DDM; FT, flow-through; W, wash; E, elution; NO TEV: same sample as the elution fraction (E) of IMAC 1; TEV: sample dialyzed overnight in the presence of TEV protease. **B**-Elution profile of MmpL3$_{Msm}$: peptidisc on size-exclusion chromatography. 1 mg of protein was incubated with the NSPr peptides at a molar ratio of 1:20. Solution was diluted to a final volume of 1 mL in buffer H and loaded on a Superdex 200 Increase 10/300 GL column and eluted in the same buffer at a flow rate of 0.35 mL min$^{-1}$ on an ÄKTA pure 25 M at 4 °C. Fractions of 0.5 mL were collected. The first peak corresponds to MmpL3$_{Msm}$:peptidisc while the second corresponds to peptidiscs in excess. Fractions between the two dash lines were analyzed by Coomassie-stained SDS-PAGE. The rightmost sample corresponds to peptidisc alone, as a control. **C**-Representative micrograph of 3 μL of sample concentrated at 3 mg mL$^{-1}$ and frozen on a holey carbon grid (Quantifoil Cu R1.2/1.3, 300 mesh).

Supernatant collected after ultracentrifugation was charged twice onto a gravity column, previously loaded with 3 mL of Nickel-Nitrilotriacetic acid (Ni-NTA) Sepharose beads (Cytiva). Two washing steps were performed with buffers D (20 mM Tris-HCl pH 8, 150 mM NaCl, 1 mM benzamidine, 10 % (v/v) glycerol, 0.5 mM β-mercaptoethanol, 20 mM imidazole, 0.026 % (w/v) DDM) and E (20 mM Tris-HCl pH 8, 1 M NaCl, 10 % (v/v) glycerol, 0.5 mM β-mercaptoethanol, 0.026 % (w/v) DDM), with 3 and 10 column volumes respectively. Tagged protein was eluted with buffer F (20 mM Tris-HCl pH 8, 200 mM NaCl, 10 % (v/v) glycerol, 0.5 mM β-mercaptoethanol, 0.026 % (w/v) DDM, 200 mM imidazole). The eluate was mixed with an excess of TEV protease at a mass ratio of 1:50 and dialyzed overnight under stirring in buffer G (20 mM Tris-HCl pH 8, 200 mM NaCl, 10 % (v/v) glycerol, 0.5 mM β-mercaptoethanol, 0.0087 % (w/v) DDM). A second IMAC was performed, by loading the dialyzed extract 3 times, leaving His-tagged materials adsorbed to nickel beads; while tag-free MmpL3$_{Msm}$-trunc was collected in the flow-through and concentrated to 6 mg mL$^{-1}$ (50 kDa cutoff Vivaspin® 20, Sartorius). The purification steps were assessed by SDS-PAGE as shown in Fig. 2.

### 2.2. Insertion of MmpL3$_{Msm}$ in peptidiscs

Peptidisc NSP$_r$ (amino acids sequence: N$_{ter}$-FAEKFKEAVKDY-FAKFWDPAAEKLKEAVKDYFAKLWD-C$_{ter}$) was obtained from Genscript with a minimum purity of 80 %. A stock solution was prepared at 6 mg mL$^{-1}$ by resuspension in water. To reconstitute MmpL3$_{Msm}$ in peptidiscs, an aliquot of 1 mg of protein in DDM was incubated for 15 min on ice with NSPr peptides solution in excess at a 1:20 M ratio. The solution was then diluted to a final volume of 1 mL with detergent-free buffer H (20 mM Tris-HCl pH 8, 150 mM NaCl, 10 % (v/v) glycerol). MmpL3$_{Msm}$: peptidisc complex was separated from free peptidiscs by size-exclusion chromatography (SEC), using a Superdex 200 Increase 10/300 GL (Cytiva) column at a flow rate of 0.35 mL min$^{-1}$ on an ÄKTA purifier at 4 °C. Fractions of 0.5 mL were collected. The purest fractions containing MmpL3$_{Msm}$:peptidisc were analyzed on SDS-PAGE, concentrated until 2.2 mg mL$^{-1}$, flash-frozen in liquid nitrogen and stored at −80 °C (Fig. 2B). At the end of the purification process, 1.7 mg of purified MmpL3$_{Msm}$ inserted in peptidiscs was obtained.

### 2.3. Cryo-EM sample preparation

MmpL3$_{Msm}$:peptidisc aliquot from −80 °C storage was thawed on ice and the buffer was exchanged using a 50 kDa cutoff Vivaspin® 20 concentration tube (Sartorius) with a glycerol-free buffer I (20 mM Tris-HCl pH 7.5, 150 mM NaCl) until concentration reached 3 mg mL$^{-1}$. 3 μL of the sample were applied onto a holey carbon grid (Quantifoil Cu R1.2/1.3, 300 mesh) that was glow-discharged for 60 s at 10 mA (EM ACE200, Leica Microsystems). Grid was blotted for 3.5 s and plunge-frozen in liquid ethane using a Vitrobot Mark IV (FEI) operated at 4 °C and 100 % humidity.

### 2.4. Cryo-EM data collection and processing

Data was collected on a 300 kV Titan Krios G2 electron microscope (FEI) equipped with a X-FEG source and a Falcon 4i direct electron detector. The energy filter was set to 10 eV width. In total 10,004 movies were recorded at 165,000x magnification and a pixel size of 0.725 Å. Each movie was exposed for 3.5 s with a total exposure dose of ~45 e$^-$/ Å$^2$ within defocus ranges from −2.5 to −0.5 μm. All data processing was done using cryoSPARC v3.3.1. Further details are shown in Fig. 3A. The movies were initially processed using cryoSPARC patch motion correction and patch CTF estimation. A total of 1,909,486 particles were bin2 extracted to a box size of 160 pixels using template-free picking with a diameter between 80 and 120 Å. After brief cleaning up with 2D classification, 1,144,545 particles were local motion corrected to a box size of 320 pixels, then 2D classified again. Particles were classified into 5 classes using *ab-initio* reconstruction followed by heterogeneous refinement. The two classified particles and volumes showing transmembrane domains were picked and further subjected to multiple rounds of 2D and 3D classifications, generating a map at a resolution of 3.4 Å. The density map was further improved by local refinement with a tight mask covering the protein region only; while surrounding peptidisc electron densities were manually removed in UCSF Chimera (v.1.16). The final volume map at an overall resolution of 3.2 Å was calculated from 348,157 particles, representing 18 % of initially extracted particles. The detailed data processing pipeline is shown in Fig. 3A.

### 2.5. Model building and refinement

The structure of MmpL3$_{Msm}$ (PDB 7K7M) obtained by X-ray crystallography was used to perform a first docking into the full EM map using *Phenix* (Liebschner et al., 2019). The model fit was improved using the *Namdinator* pipeline (Kidmose et al., 2019). The structure was then manually adjusted into the EM density modified map with Coot (Casañal et al., 2020) and refined using the *real.space.refine* module of *Phenix*. Structure validation was performed with *Phenix* and the MolProbity server (Williams et al., 2018).

## 3. Results and discussion

MmpL3$_{Msm}$ (Fig. 1) was recombinantly expressed in *E. coli*, purified to high purity and homogeneity and reconstituted in peptidiscs with a three-step chromatography procedure (Fig. 2) with only slight modifications as compared to the previously reported protocol (Ung et al., 2022a). After reconstitution into peptidiscs, the protein was purified by size-exclusion chromatography (SEC) using a Superdex 200 Increase10/300 GL column enabling separation of MmpL3$_{Msm}$ from excess of peptidiscs as compared to the less resolved Superose 6 Increase 10/300 GL column we previously used (Ung et al., 2022a).

A high-quality cryo-EM dataset (Table I) was collected and processed to a resolution of 3.4 Å (Fig. 3A) (Map 1) and the map was further improved through density modification (Map 2) to an overall resolution of 3.2 Å (Fig. 3A and B). Generally, the cryo-EM map was well defined with the local resolution ranging from 3 Å to 5 Å, and with nearly all parts of the model being visible (Fig. 4A and B). We could model residues 1 to 738 from our initial construct meaning that only the first methionine and the last 40 amino acids in the C-terminus (which includes a TEV cleavage site) were not seen. In addition, amino acids 376 to 383 were not modeled, which are part of a linker (see more later) in between the two subdomains of the transmembrane domain, known as the MMPL domains. These non-modeled regions were also missing or partly missing in the former MmpL3 structures. The two MMPL domains were particularly well defined in the cryo-EM density with local resolution ranging from 3 to 3.2 Å resolution. We could unambiguously rebuild and assign side chains for almost all residues of the twelve transmembrane helices (Fig. 4C). The two extracellular domains, denoted periplasmic domain 1 and 2 or PD1 and PD2, are well defined as seen on the local resolution map (Fig. 4A). We did not identify any additional density associated with PD1 or PD2 supporting the presence of endogenous *E. coli* lipids as previously reported (Su et al., 2019), implying our structure represents an apo state of MmpL3$_{Msm}$.

Finally, another indication of the cryo-EM map quality is the clear presence of several alpha-helices surrounding MmpL3$_{Msm}$. These extra helices were attributed to peptidisc peptides that embed the MmpL3$_{Msm}$ transmembrane domains. The peptidisc is arranged into two to three layers of helices arranged perpendicular to the helices of the MMPL domains (Fig. 4D). We did not build these helices in the final model deposited to the PDB as the side chains and helices orientation could not be assigned with high confidence. Similar observations were described for the MsbA ABC transporter cryo-EM structure reconstituted in peptidiscs (Angiulli et al., 2020).

MmpL3$_{Msm}$ reconstituted into peptidiscs is a monomer as observed
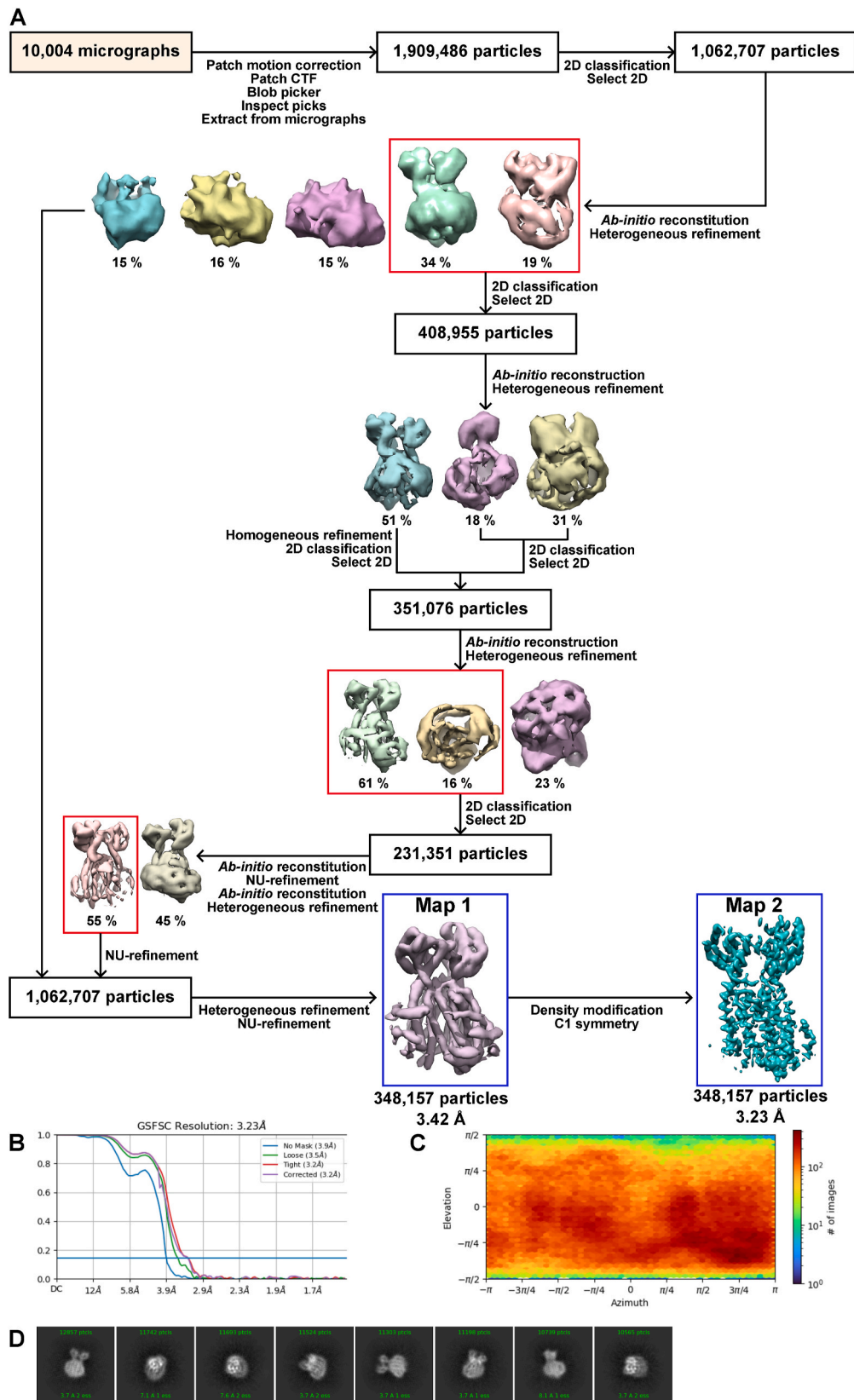
**Fig. 3.** Cryo-EM data processing pipeline on cryoSPARC

**A**-Overview of the processing steps, leading to an electron density map at an overall resolution of 3.4 Å (Map 1) further improved by density modification to an overall resolution of 3.2 Å (Map 2), and made with 18 % of the initially extracted particles. **B**-Gold Standard Fourier Shell Correlation curve of Map 2. **C**-Direction distribution. **D**-Representative 2D classification averages. (For interpretation of the references to color in this figure legend, the reader is referred to the Web version of this article.)

**Table 1**

Data processing, refinement and model statistics.

| Structure | MmpL3$_{Msm}$::peptidisc |
|---|---|
| EMDB accession code | 18464 |
| PDB accession code | 8QKK |
| **Data collection** | |
| EM equipment | Titan Krios™ G2 |
| Voltage (kV) | 300 |
| Source | X-FEG |
| Magnification | 165,000 |
| Detector | Falcon 4i |
| Data collection mode | NanoProbe |
| Pixel size (Å) | 0.725 |
| Energy filter width (eV) | 10 |
| Total exposure dose (e$^-$/Å$^2$) | 45 |
| Defocus range (μm) | −2.5–−0.5 |
| Total exposure time (s) | 3.5 |
| | |
| **Data processing** | |
| Software | cryoSPARC v3.3.1 |
| Number of fractions | 45 |
| Number of initial micrographs | 10,004 |
| Number of initial particles | 1,909,486 |
| Number of final particles | 348,157 |
| Symmetry | C1 |
| Resolution (Å) | 3.23 |
| FSC threshold | 0.143 |
| | |
| **Refinement** | |
| Initial model used (PDB ID) | 7K7M |
| Model resolution cut-off (Å) | |
| Number of protein residues | 730 |
| Nonhydrogen atoms | 5581 |
| RMSD[a] | |
| Bond lengths (Å) | 0.004 |
| Bond angles (°) | 0.953 |
| ADP (B-factors) min/max/mean | 8.3/127.4/56.5 |
| Model vs. Data | |
| CC (mask)/(box)/(peak)/(volume) | 0.79/0.62/0.58/0.75 |
| **Validation** | |
| MolProbity score | 1.64 |
| Clash score | 9 |
| Rotamers outliers (%) | 0 |
| Ramachandran plot (%) | |
| Favored (%) | 97.11 |
| Allowed (%) | 2.89 |
| Disallowed (%) | 0 |

[a] Root Mean Square Deviation.

for previous structures of mycobacterial MmpL3. The structure can be divided into four main domains. The first MMPL domain (MMPL1), residues 1–36 and 172–341, is composed of six transmembrane helices separated by PD1 encompassing residues 37–171 and between TM1 and TM2. The second MMPL domain (MMPL2) contains six transmembrane helices and is formed by residues 400–427 and 549–730. PD2 associated with MMPL2 is established by residues 428–548 and is situated between TM7 and TM8. The two MMPL domains are separated by a linker formed by amino acids 342–399, creating a long transversal helix along the membrane interface on the cytoplasmic side, and one flexible region which only have been visualized in two MmpL3$_{Msm}$ structures so far, most of which most have been modeled in our structure (Su et al., 2021).

To validate the peptidisc strategy as a solid alternative to investigate MmpL3 structure, it was crucial to address the preservation of its structural integrity in this condition. Structural comparison demonstrates that our MmpL3$_{Msm}$ structure inserted into peptidiscs is comparable with structures formerly solved either in their apo- or ligand-bound states i.e. with lipids, glycolipids, or MmpL3 inhibitors (Su et al., 2019, 2021; Zhang et al., 2019). Superposition of our structure on the structure of MmpL3 bound to TMM (PDB: 7N6B, determined using cryo-EM), on the MmpL3-phosphatidylethanolamine complex (PDB: 6OR2, X-ray crystallography) and on a MmpL3 apo structure (PDB: 6AJF, X-ray crystallography) suggests a high structural similarity with RMSDs of 0.64, 0.83 and 0.76 Å, respectively. This observation strongly indicates that peptidisc-stabilization preserves the structural integrity of MmpL3$_{Msm}$ as no major structural rearrangement could be noticed.

Interestingly, our MmpL3$_{Msm}$ structure reveals a new configuration of the linker inbetween MMPL1 and MMPL2 (Fig. 5C). Although less defined than other parts of the model, the cryo-EM map enables us to place the two helices of the linker region without any ambiguity. The linker forms a helical hairpin and dips into the membrane from the cytosolic side, despite several charged residues. This is different from the arrangement of the linker in the previous structures (Su et al., 2021) in which this region could be observed (Fig. 5C). In our structure, the helical hairpin is close to TM1, TM2 and TM3 which is similar yet distinct to the X-ray structure (PDB: 7K7M) bound to trehalose 6-decanoate (T6D), a detergent mimicking TMM. Conversely, in a nanodisc-stabilized cryo-EM structure bound to TMM (PDB: 7N6B), the feature does not enter the membrane region, and is rather found at the membrane interface, prolonging the transversal helix. This observation indicates that the helical hairpin may adopt a tight configuration associated with TM1, TM2 and TM3 in the absence of TMM, and conversely, that it may adapt a more relaxed conformation upon ligand binding. Alternatively, the conditions exploited for the nanodisc-stabilized structure are incompatible with membrane insertion of the helical hairpin. The new structure may therefore have identified a novel structural rearrangement of the linker region but we cannot, however, rule out that the movement is not induced by the presence of the peptidiscs surrounding MmpL3. Further work to confirm these observations will be needed. Notably, the determination of the structure of MmpL3 reconstituted into peptidiscs and bound to TMM would be of great interest to fully apprehend the above-described structural change.

To conclude, this study demonstrates the possibility of investigating MmpL3$_{Msm}$ structure in an environment free of lipid or detergent and compatible with the acquisition of high-quality cryo-EM data. This work demonstrates that under these conditions the native structure of MmpL3$_{Msm}$ is preserved. Further, the new approach permitted to identify the linker region in a new conformation not previously observed. As the peptidisc technology is easy to implement, it may enhance the possibilities to further investigate MmpL3. Notably, several binding partners of MmpL3 were recently discovered but their functional role (Belardinelli et al., 2019; Fay et al., 2019; Melly et al., 2019) and how they interact with MmpL3 remains to be elucidated. Some of these partners are membrane proteins such as the two essential proteins TtfA (Fay et al., 2019; Ung et al., 2020) or TmaT (Belardinelli et al., 2016) or the soluble protein LpqN (Melly et al., 2019). We foresee that the use of peptidiscs could be of peculiar interest for the structural investigation of these complexes as one advantage of this method is the absence of limitation in terms of the size of the particle that can be inserted. Additionally, since no detergent is needed the peptidisc strategy could also be more compatible to reconstitute complex(es) formed between MmpL3 and soluble proteins.

### Funding information

### CRediT authorship contribution statement

**Julie Couston:** Investigation, Data curation, Formal analysis, Visualization, Writing – original draft. **Zongxin Guo:** Investigation, Data curation, Formal analysis, Visualization, Writing – review & editing. **Kaituo Wang:** Data curation, Formal analysis, Writing – review &
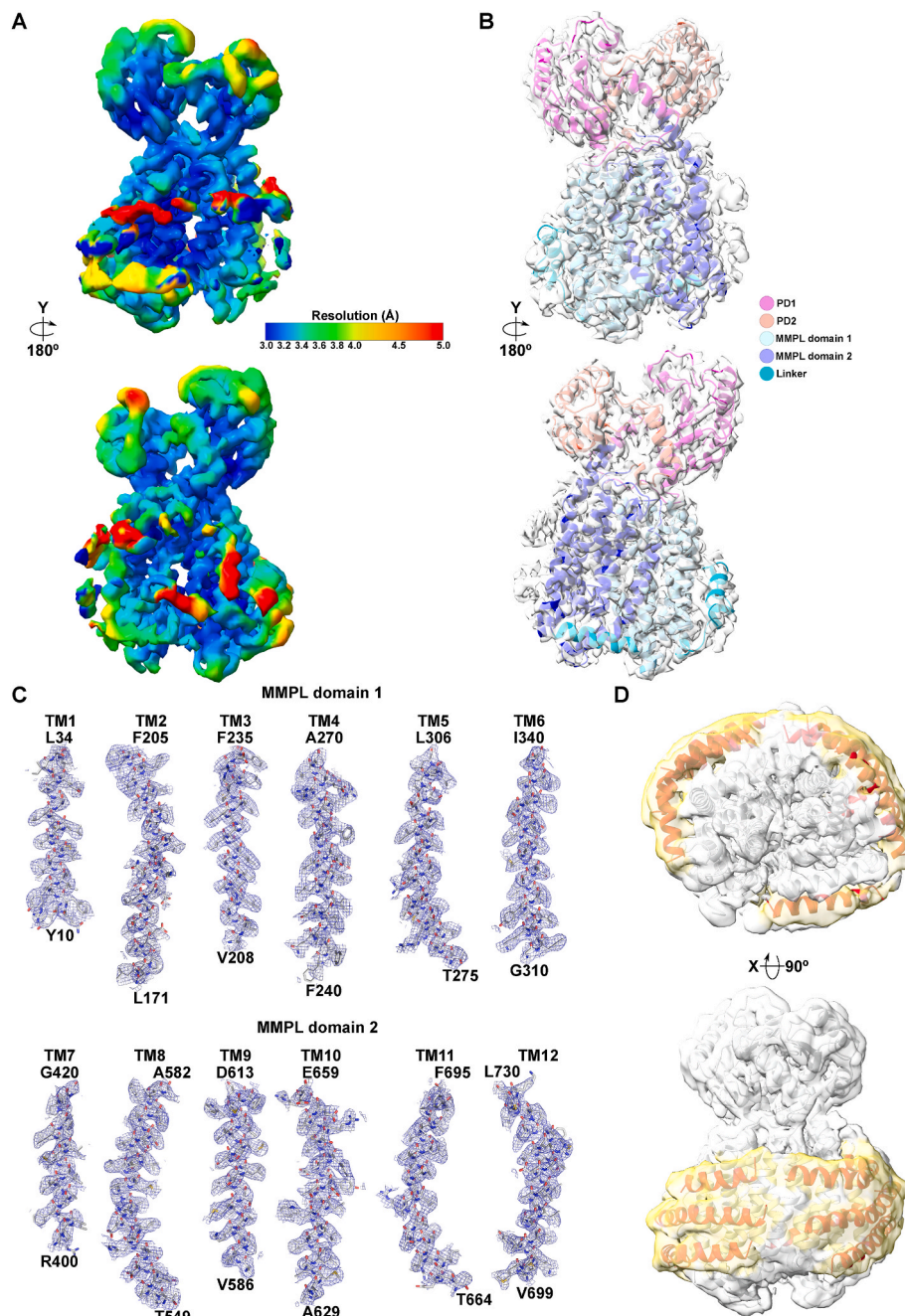
**Fig. 4.** Cryo-EM maps quality and model building

**A-**The local resolution map ranging from 3 to 5 Å resolution was calculated with cryoSPARC. The map attests that the highest resolution (dark blue) correlates with the transmembrane helices. The map contour (level 0.21 in ChimeraX) was adjusted so that the peptidisc peptides are not visible. **B-**The map at 3.2 Å (Map 2) resolution is represented as a white transparent surface. The MmpL3$_{Msm}$ model fitted in the map is represented as a cartoon and colored according to the different domains. PD1 and PD2 stand for periplasmic domains 1 and 2. MMPL domain 1 encompasses the transmembrane helices 1 to 6 while MMPL domain 2 is composed of helices 7 to 12. The linker region separates the two MMPL domains. The map contour is 0.33 and displayed in ChimeraX. **C-**Representation of the EM map. The 3.2 Å resolution map (Map 2) is shown as a blue mesh and contoured (level 5 σ in PyMOL) around each transmembrane helix (TM) and represented as sticks. **D-**EM map (Map 1, level 0.12 in ChimeraX) attesting the presence of peptides from the peptidisc. The helical peptides surrounding MmpL3$_{Msm}$ are shown as red cartoons while the corresponding EM map is depicted as a yellow transparent surface. Almost all the TM parts of MmpL3$_{Msm}$ are embedded into peptidiscs apart from the linker region. (For interpretation of the references to color in this figure legend, the reader is referred to the Web version of this article.)

## Declaration of competing interest
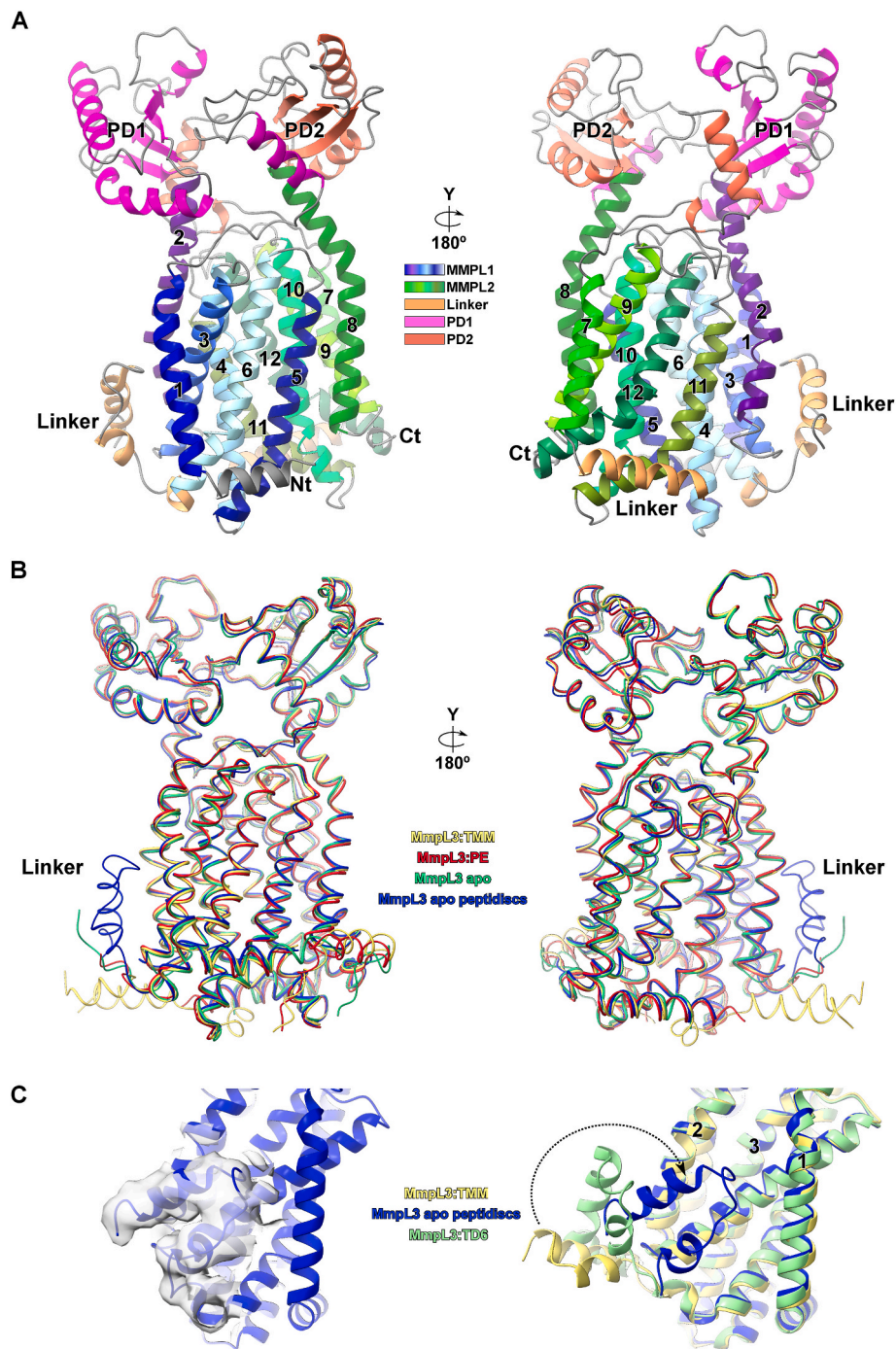
**Fig. 5.** Reconstitution of MmpL3$_{Msm}$ into peptidiscs preserves its structure.
**A-**Depiction of the final model of MmpL3$_{Msm}$. The model is represented as cartoons. The two periplasmic domains PD1 and PD2 are colored in magenta and coral and each transmembrane helix is annotated and displayed with a specific color. The linker region (residues 342–399) could only be partly rebuilt (376–383 are missing) and is represented in sandy brown. **B-**Comparison of MmpL3$_{Msm}$ reconstituted into peptidiscs with other MmpL3 structures. The structures represented as ribbons were superposed using ChimeraX. MmpL3$_{Msm}$ bound to TMM (PDB: 7N6B) is in yellow, MmpL3$_{Msm}$ bound to phosphatidylethanolamine (PE) (PDB: 6OR2) in red and the MmpL3$_{Msm}$ apo structure (PDB: 6AJF) in green while MmpL3$_{Msm}$ structure into peptidiscs is in blue. **C-** Comparison of the linker region conformation in the TMM (PDB: 7N6B) and T6D (PDB: 7K7M) bound structures with the one in the apo structure. The EM map (Map 1 contoured at 0.169 in ChimeraX) is well defined for the linker region. In the absence of ligand, the linker is closer to TM1, 2 and 3 while it is in an open conformation when MmpL3 is bound to its substrates. (For interpretation of the references to color in this figure legend, the reader is referred to the Web version of this article.)

## Data availability

Data will be made available on request.

Montpellier for fruitful discussions and support.

## References

Abrahams, K.A., Besra, G.S., 2018. Mycobacterial cell wall biosynthesis: a multifaceted antibiotic target. Parasitology 145, 116–133. https://doi.org/10.1017/S0031182016002377.

Adams, O., Deme, J.C., Parker, J.L., , CRyPTIC Consortium, Fowler, P.W., Lea, S.M., Newstead, S., 2021. Cryo-EM structure and resistance landscape of M. tuberculosis MmpL3: an emergent therapeutic target, 1993 Struct. Lond. Engl. 29, 1182–1191. https://doi.org/10.1016/j.str.2021.06.013. e4.

Alav, I., Kobylka, J., Kuth, M.S., Pos, K.M., Picard, M., Blair, J.M.A., Bavro, V.N., 2021. Structure, assembly, and function of tripartite efflux and type 1 secretion systems in gram-negative bacteria. Chem. Rev. 121, 5479–5596. https://doi.org/10.1021/acs.chemrev.1c00055.

Angiulli, G., Dhupar, H.S., Suzuki, H., Wason, I.S., Duong Van Hoa, F., Walz, T., 2020. New approach for membrane protein reconstitution into peptidiscs and basis for their adaptability to different proteins. Elife 9, e53530. https://doi.org/10.7554/eLife.53530.

Belardinelli, J.M., Stevens, C.M., Li, W., Tan, Y.Z., Jones, V., Mancia, F., Zgurskaya, H.I., Jackson, M., 2019. The MmpL3 interactome reveals a complex crosstalk between cell envelope biosynthesis and cell elongation and division in mycobacteria. Sci. Rep. 9, 10728 https://doi.org/10.1038/s41598-019-47159-8.

Belardinelli, J.M., Yazidi, A., Yang, L., Fabre, L., Li, W., Jacques, B., Angala, S.K., Rouiller, I., Zgurskaya, H.I., Sygusch, J., Jackson, M., 2016. Structure-function profile of MmpL3, the essential mycolic acid transporter from Mycobacterium tuberculosis. ACS Infect. Dis. 2, 702–713. https://doi.org/10.1021/acsinfecdis.6b00095.

Carlson, M.L., Young, J.W., Zhao, Z., Fabre, L., Jun, D., Li, Jianing, Li, Jun, Dhupar, H.S., Wason, I., Mills, A.T., Beatty, J.T., Klassen, J.S., Rouiller, I., Duong, F., 2018. The Peptidisc, a simple method for stabilizing membrane proteins in detergent-free solution. Elife 7, e34085. https://doi.org/10.7554/eLife.34085.

Casañal, A., Lohkamp, B., Emsley, P., 2020. Current developments in Coot for macromolecular model building of electron cryo-microscopy and crystallographic data. Protein Sci. Publ. Protein Soc. 29, 1069–1078. https://doi.org/10.1002/pro.3791.

Denisov, I.G., Sligar, S.G., 2017. Nanodiscs in membrane biochemistry and biophysics. Chem. Rev. 117, 4669–4713. https://doi.org/10.1021/acs.chemrev.6b00690.

Dulberger, C.L., Rubin, E.J., Boutte, C.C., 2020. The mycobacterial cell envelope — a moving target. Nat. Rev. Microbiol. 18, 47–59. https://doi.org/10.1038/s41579-019-0273-7.

Dupont, C., Viljoen, A., Dubar, F., Blaise, M., Bernut, A., Pawlik, A., Bouchier, C., Brosch, R., Guérardel, Y., Lelièvre, J., Ballell, L., Herrmann, J.-L., Biot, C., Kremer, L., 2016. A new piperidinol derivative targeting mycolic acid transport in Mycobacterium abscessus. Mol. Microbiol. 101, 515–529. https://doi.org/10.1111/mmi.13406.

Fay, A., Czudnochowski, N., Rock, J.M., Johnson, J.R., Krogan, N.J., Rosenberg, O., Glickman, M.S., 2019. Two accessory proteins govern MmpL3 mycolic acid transport in mycobacteria. mBio 10, e00850. https://doi.org/10.1128/mBio.00850-19, 19.

Frauenfeld, J., Löving, R., Armache, J.-P., Sonnen, A.F.-P., Guettou, F., Moberg, P., Zhu, L., Jegerschöld, C., Flayhan, A., Briggs, J.A.G., Garoff, H., Löw, C., Cheng, Y., Nordlund, P., 2016. A saposin-lipoprotein nanoparticle system for membrane proteins. Nat. Methods 13, 345–351. https://doi.org/10.1038/nmeth.3801.

Grzegorzewicz, A.E., Pham, H., Gundi, V.A.K.B., Scherman, M.S., North, E.J., Hess, T., Jones, V., Gruppo, V., Born, S.E.M., Korduláková, J., Chavadi, S.S., Morisseau, C., Lenaerts, A.J., Lee, R.E., McNeil, M.R., Jackson, M., 2012. Inhibition of mycolic acid transport across the Mycobacterium tuberculosis plasma membrane. Nat. Chem. Biol. 8, 334–341. https://doi.org/10.1038/nchembio.794.

Hu, T., Yang, Xiaolin, Liu, F., Sun, S., Xiong, Z., Liang, J., Yang, Xiaobao, Wang, H., Yang, Xiuna, Guddat, L.W., Yang, H., Rao, Z., Zhang, B., 2022. Structure-based design of anti-mycobacterial drug leads that target the mycolic acid transporter MmpL3, 1993 Struct. Lond. Engl. 30, 1395–1402. https://doi.org/10.1016/j.str.2022.07.009. e4.

Kidmose, R.T., Juhl, J., Nissen, P., Boesen, T., Karlsen, J.L., Pedersen, B.P., 2019. Namdinator - automatic molecular dynamics flexible fitting of structural models into cryo-EM and crystallography experimental maps. IUCrJ 6, 526–531. https://doi.org/10.1107/S2052252519007619.

Liebschner, D., Afonine, P.V., Baker, M.L., Bunkóczi, G., Chen, V.B., Croll, T.I., Hintze, B., Hung, L.-W., Jain, S., McCoy, A.J., Moriarty, N.W., Oeffner, R.D., Poon, B.K., Prisant, M.G., Read, R.J., Richardson, J.S., Richardson, D.C., Sammito, M.D., Sobolev, O.V., Stockwell, D.H., Terwilliger, T.C., Urzhumtsev, A.G., Videau, L.L., Williams, C.J., Adams, P.D., 2019. Macromolecular structure determination using X-rays, neutrons and electrons: recent developments in Phenix. Acta Crystallogr. Sect. Struct. Biol. 75, 861–877. https://doi.org/10.1107/S2059798319011471.

Marrakchi, H., Lanéelle, M.-A., Daffé, M., 2014. Mycolic acids: structures, biosynthesis, and beyond. Chem. Biol. 21, 67–85. https://doi.org/10.1016/j.chembiol.2013.11.011.

Melly, G.C., Stokas, H., Dunaj, J.L., Hsu, F.F., Rajavel, M., Su, C.-C., Yu, E.W., Purdy, G. E., 2019. Structural and functional evidence that lipoprotein LpqN supports cell envelope biogenesis in Mycobacterium tuberculosis. J. Biol. Chem. 294, 15711–15723. https://doi.org/10.1074/jbc.RA119.008781.

Nikaido, H., 2018. RND transporters in the living world. Res. Microbiol. 169, 363–371. https://doi.org/10.1016/j.resmic.2018.03.001.

North, E.J., Schwartz, C.P., Zgurskaya, H.I., Jackson, M., 2023. Recent advances in mycobacterial membrane protein large 3 inhibitor drug design for mycobacterial infections. Expet Opin. Drug Discov. 18, 707–724. https://doi.org/10.1080/17460441.2023.2218082.

Quémard, A., 2016. New insights into the mycolate-containing compound biosynthesis and transport in mycobacteria. Trends Microbiol. 24, 725–738. https://doi.org/10.1016/j.tim.2016.04.009.

Stevens, C.M., Babii, S.O., Pandya, A.N., Li, W., Li, Y., Mehla, J., Scott, R., Hegde, P., Prathipati, P.K., Acharya, A., Liu, J., Gumbart, J.C., North, J., Jackson, M., Zgurskaya, H.I., 2022. Proton transfer activity of the reconstituted Mycobacterium tuberculosis MmpL3 is modulated by substrate mimics and inhibitors. Proc. Natl. Acad. Sci. U.S.A. 119, e2113963119 https://doi.org/10.1073/pnas.2113963119.

Su, C.-C., Klenotic, P.A., Bolla, J.R., Purdy, G.E., Robinson, C.V., Yu, E.W., 2019. MmpL3 is a lipid transporter that binds trehalose monomycolate and phosphatidylethanolamine. Proc. Natl. Acad. Sci. U.S.A. 116, 11241–11246. https://doi.org/10.1073/pnas.1901346116.

Su, C.-C., Klenotic, P.A., Cui, M., Lyu, M., Morgan, C.E., Yu, E.W., 2021. Structures of the mycobacterial membrane protein MmpL3 reveal its mechanism of lipid transport. PLoS Biol. 19, e3001370 https://doi.org/10.1371/journal.pbio.3001370.

Tahlan, K., Wilson, R., Kastrinsky, D.B., Arora, K., Nair, V., Fischer, E., Barnes, S.W., Walker, J.R., Alland, D., Barry, C.E., Boshoff, H.I., 2012. SQ109 targets MmpL3, a membrane transporter of trehalose monomycolate involved in mycolic acid donation to the cell wall Core of. Mycobacterium tuberculosis. Antimicrob. Agents Chemother. 56, 1797–1809. https://doi.org/10.1128/AAC.05708-11.

Ung, K.L., Alsarraf, H., Kremer, L., Blaise, M., 2022a. MmpL3, the trehalose monomycolate transporter, is stable in solution in several detergents and can be reconstituted into peptidiscs. Protein Expr. Purif. 191, 106014 https://doi.org/10.1016/j.pep.2021.106014.

Ung, K.L., Alsarraf, H.M.A.B., Kremer, L., Blaise, M., 2020. The crystal structure of the mycobacterial trehalose monomycolate transport factor A, TtfA, reveals an atypical fold. Proteins 88, 809–815. https://doi.org/10.1002/prot.25863.

Ung, K.L., Winkler, M., Schulz, L., Kolb, M., Janacek, D.P., Dedic, E., Stokes, D.L., Hammes, U.Z., Pedersen, B.P., 2022b. Structures and mechanism of the plant PIN-FORMED auxin transporter. Nature 609, 605–610. https://doi.org/10.1038/s41586-022-04883-y.

Viljoen, A., Dubois, V., Girard-Misguich, F., Blaise, M., Herrmann, J.-L., Kremer, L., 2017. The diverse family of MmpL transporters in mycobacteria: from regulation to antimicrobial developments. Mol. Microbiol. 104, 889–904. https://doi.org/10.1111/mmi.13675.

Who, 2022. Global Tuberculosis Report 2022 [WWW Document]. URL. https://www.who.int/teams/global-tuberculosis-programme/tb-reports/global-tuberculosis-report-2022.

Williams, C.J., Headd, J.J., Moriarty, N.W., Prisant, M.G., Videau, L.L., Deis, L.N., Verma, V., Keedy, D.A., Hintze, B.J., Chen, V.B., Jain, S., Lewis, S.M., Arendall, W.B., Snoeyink, J., Adams, P.D., Lovell, S.C., Richardson, J.S., Richardson, D.C., 2018. MolProbity: more and better reference data for improved all-atom structure validation. Protein Sci. Publ. Protein Soc. 27, 293–315. https://doi.org/10.1002/pro.3330.

Xu, Z., Meshcheryakov, V.A., Poce, G., Chng, S.-S., 2017. MmpL3 is the flippase for mycolic acids in mycobacteria. Proc. Natl. Acad. Sci. U.S.A. 114, 7993–7998. https://doi.org/10.1073/pnas.1700062114.

Yang, Xiaolin, Hu, T., Yang, Xiuna, Xu, W., Yang, H., Guddat, L.W., Zhang, B., Rao, Z., 2020. Structural basis for the inhibition of mycobacterial MmpL3 by NITD-349 and SPIRO. J. Mol. Biol. 432, 4426–4434. https://doi.org/10.1016/j.jmb.2020.05.019.

Zhang, B., Li, J., Yang, Xiaolin, Wu, L., Zhang, J., Yang, Y., Zhao, Y., Zhang, L., Yang, Xiuna, Yang, Xiaobao, Cheng, X., Liu, Z., Jiang, B., Jiang, H., Guddat, L.W., Yang, H., Rao, Z., 2019. Crystal structures of membrane transporter MmpL3, an anti-TB drug target. Cell 176, 636–648. https://doi.org/10.1016/j.cell.2019.01.003 e13.